CHAPTER V

Some Numerical Methods for Discontinuous Flows in Porous Media

PHILLIP COLELLA, PAUL CONCUS, AND JAMES SETHIAN

1. Introduction. The numerical modeling of fluid displacement through a porous medium has received increased attention in recent years. Interest has been stimulated by the development of enhanced recovery methods for obtaining petroleum from underground reservoirs and the advent of larger, higher-speed computers. A common feature found in most important recovery methods is the propagation of fronts that are steep or discontinuous. Examples of such fronts are those involving different fluids, such as in the waterflooding of a petroleum reservoir, or between regions of differing concentrations, as in some tertiary recovery processes. Even though steep fronts may not be present initially, they can develop naturally in time as a consequence of the inherent nonlinearity of fluid displacement in porous media.

Accurate following of steep fronts numerically can pose substantial difficulty for conventional discretization methods, which rely on underlying assumptions on smoothness of solutions. In an attempt to overcome these difficulties, a study was initiated several years ago in the Mathematics Group of the Lawrence Berkeley Laboratory to develop high-resolution numerical methods for solving the equations of flow through a porous medium. A discussion of this study is given here with emphasis on the details of newer directions being pursued. Included as well is some introductory background material given in an earlier, less-detailed review [14].

Our study centers on numerical methods that incorporate analytical information concerning the propagation of discontinuities in a flow. Such methods have been effective in treating hyperbolic conservation laws arising in gas dynamics and can be adapted in many cases to the equations of porous flow. The initial parts of the study focused on the random choice method, a method that can track solution discontinuities sharply and accurately in one space dimension. The method represents a solution by a piecewise constant approximation and uses Riemann problem solutions and a sampling procedure to advance in time. As a first step this method was adapted to solving the Buckley–Leverett equation for immiscible displacement in one space dimension. Extensions to more than one

space dimension were carried out subsequently by means of operator splitting (§3).

Because of inaccuracies that may be introduced for some problems at discontinuity fronts propagating obliquely to the splitting directions, investigations of alternatives were initiated for multidimensional cases. A front tracking method for multidimensional problems was developed based on the SLIC scheme introduced in [26]. The method assigns to mesh cells a value representing the fraction of the cell lying behind the front, and the cell fractions are then appropriately advanced at each time step (§4). Two other methods, currently under investigation, are a higher order version of Godunov's method that utilizes piecewise linear rather than piecewise constant segments for constructing conservative fluxes (§5), and a method based on an improved splitting procedure, which will be reported in [9].

2. Equations for immiscible displacement. We consider the simultaneous, immiscible flow of two incompressible fluids in an isotropic, homogeneous porous medium. We do not include the effects of capillary pressure, thus propagating fronts will be sharp. For a region whose interior is free of sources and sinks (i.e., injection or production wells), one is led to the equations [28]

$$\phi \frac{\partial s}{\partial t} + \mathbf{q} \cdot \nabla f(s) - \gamma \frac{\partial}{\partial z} g(s) = 0, \tag{2.1}$$

$$\nabla \cdot \mathbf{q} = Q, \tag{2.2}$$

$$\mathbf{q} = -\lambda(s)[\nabla p - \gamma \tilde{g}(s)\mathbf{e}_k]. \tag{2.3}$$

In the above equations $s(\mathbf{x}, t)$, $0 \leq s \leq 1$, is the saturation of the wetting fluid (fraction of available pore volume occupied by the fluid). The saturation of the nonwetting fluid is then $1 - s$. The independent variables $\mathbf{x}$ and t are space and time, respectively, and $\mathbf{q}(\mathbf{x}, t)$ is the total velocity (sum of the individual velocities of the two fluids). If gravity is present it is assumed to act in the negative z direction, with $\mathbf{e}_k$ the unit vector in the positive z direction. The quantity $p(\mathbf{x}, t)$ is the excess over gravitational head of the reduced pressure; here the reduced pressure is the average of the individual phase pressures less the gravitational head. The quantity Q represents the sources and sinks of fluid on the boundary of the domain, and ϕ is the porosity, which will be assumed constant. The quantity γ, the coefficient of the gravitational term, is the product of the acceleration due to gravity times the density difference between the wetting and nonwetting phases.

Equation (2.1) is the Buckley–Leverett equation, which for a given $\mathbf{q}$ is hyperbolic. Equation (2.2) is the incompressibility condition, and (2.3) is Darcy's law. For a given s, (2.2), (2.3) is elliptic.

The functions of saturation $f(s)$, $g(s)$, $\lambda(s)$, and $\tilde{g}(s)$ can be expressed in terms

of the empirically determined phase mobilities (ratios of permeability to viscosity) λ_n and λ_w of the nonwetting and wetting fluids. For immiscible displacement these are

$$f(s) = \lambda_w/\lambda, \qquad g(s) = \lambda_n f,$$
$$\tilde{g}(s) = \lambda_n/\lambda, \qquad \lambda(s) = \lambda_n + \lambda_w.$$

The quantities f, g, and $\tilde{g}$ are nonnegative, and λ is positive.

A distinguishing feature of the immiscible displacement equations is that f and g are nonconvex. Typically f has one inflection, as depicted for a model case in Fig. 1, and g has two, as depicted in Fig. 2. Thus weak solutions may have combinations of propagating shock and expansion waves in contact.

Attempts to solve (2.1), (2.2), (2.3), subject to appropriate boundary conditions, by standard discretization methods such as finite difference or finite element methods can give rise to substantial difficulty. Inaccuracies may arise near a moving front, or an incorrect weak solution may be obtained. To circumvent these difficulties, the first phase of our study initiated an attempt to adapt the random choice method to solving problems of fluid displacement in porous media.

3. Random choice method. The random choice method, which was formulated originally for solving the equations of gas dynamics, is a numerical method incorporating the accurate propagation of solution discontinuities. It is based on a mathematical construction of Glimm [17] that was developed into a practical

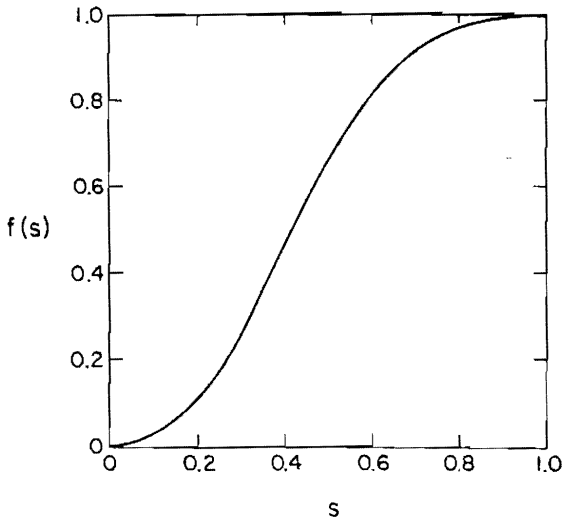

FIG. 1.

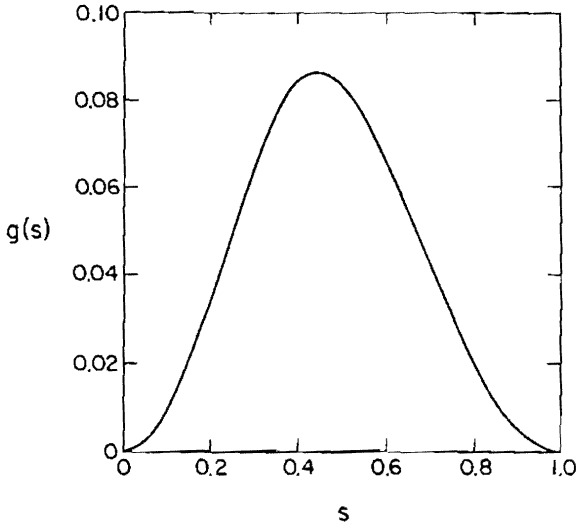

FIG. 2.

and efficient computation algorithm by Chorin [6], [7]. It was first adapted to porous flow problems in [15], and applied extensively in [18] and related papers.

For a single nonlinear conservation law

$$\frac{\partial s}{\partial t} + \frac{\partial}{\partial z}\psi(s) = 0, \tag{3.1}$$

to which (2.1) reduces in one space dimension, the random choice method advances a solution in time as follows. The solution $s(z,t_n)$ at time t_n is represented by a piecewise constant function on a spatial grid of spacing Δz, with the function equal to $s_i^n = s(z_i, t_n)$ in the interval $z_i - \frac{1}{2}\Delta z < z \leq z_i + \frac{1}{2}\Delta z$. An exact solution of (3.1) is constructed analytically by the method of characteristics for this piecewise constant initial data by solving the collection of Riemann problems: (3.1) with initial data

$$s(z, t_n) = \begin{cases} s_i^n, & z \leq z_i + \frac{1}{2}\Delta z, \\ s_{i+1}^n, & z > z_i + \frac{1}{2}\Delta z. \end{cases} \tag{3.2}$$

As long as the time increments Δt satisfy the Courant–Friedrichs–Lewy condition $(\Delta t/\Delta z) \cdot \max|\psi'(s)| < \frac{1}{2}$ (or <1 for forms of the method using half time steps on staggered grids), the waves propagating from the individual mesh-point discontinuities will not interact during a given time step. This permits the solution of (3.1) to be obtained during the step by joining together the separate Riemann problem solutions.

The above technique of obtaining the exact solution is common to other methods, such as Godunov's method. What distinguishes the random choice method is that the piecewise constant representation of the solution s is constructed at the new time by sampling the exact solution at a point within each spatial interval. In this way moving discontinuities remain perfectly sharp (since no intermediate values are introduced by the method), at the price of introducing a small amount of uncertainty into the position of the waves.

The sampling procedure for the random choice method should be equidistributed to yield an accurate representation of the solution [7], [10]. The deterministic van der Corput sequence proposed in [10] has been found to be particularly well suited for the method. The mth number θ_m in the basic sequence is given by

$$\theta_m = \sum_{k=0}^{M} i_k 2^{-(k+1)},$$

where the binary expansion for m is

$$m = \sum_{k=0}^{M} i_k 2^k.$$

Extensions for use with multidimensional problems are given in [10].

The random choice method is essentially first order and is observed to give good results for one-dimensional problems.

3.1 Riemann problems. The practicality of the random choice method depends on being able to solve the Riemann problems efficiently. For the immiscible displacement problem the function $\psi(s)$, which is a linear combination of $f(s)$ and $g(s)$, has either one or two inflections, depending on the relative magnitudes of q and γ. If the gravity term $\gamma g(s)$ in (2.1) is small compared with the transport term $qf(s)$, then there is only one inflection in $\psi(s)$ (as in $f(s)$ in

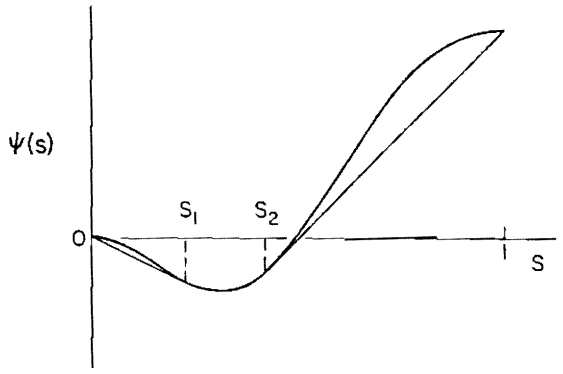

FIG. 3.

Fig. 1), for which case the Riemann problem solution is given in [15]. For the case of two inflections in $\psi(s)$ the solution is given in [1], [4], and for a special case in [29].

A typical example for which two inflections occur is depicted in Fig. 3, which is taken from [4]. The Riemann problem solution is obtained by applying the following general conditions, which must hold along any curve of discontinuity of $s(z, t)$: Let $s_- = \lim_{z \to z_-} s(z, t)$ and $s_+ = \lim_{z \to z_+} s(z, t)$ be the limiting values from the left and right, respectively, at a discontinuity. Then there must hold (see [24], [27]):

(i) *Rankine–Hugoniot jump condition.* The curve of discontinuity is a straight line with slope

$$\frac{dz}{dt} = \frac{\psi(s_+) - \psi(s_-)}{s_+ - s_-}.$$

(ii) *Generalized entropy condition.* For any s between s_+ and s_- there holds

$$\frac{\psi(s_+) - \psi(s)}{s_+ - s} \geqq \frac{\psi(s_+) - \psi(s_-)}{s_+ - s_-}.$$

For the case $s_i^n = 0$ and $s_{i+1}^n = 1$, one obtains the solution of (3.1), (3.2) depicted in Fig. 4. Figure 3 depicts the corresponding concave hull of $\psi(s)$, whose points of tangency with $\psi(s)$ determine the shock propagation speeds. The two shocks shown in Fig. 4 propagate to the left and right, respectively, from the initial discontinuity. The characteristics from the left of the discontinuity intersect the leftward travelling shock, and those from the right intersect the

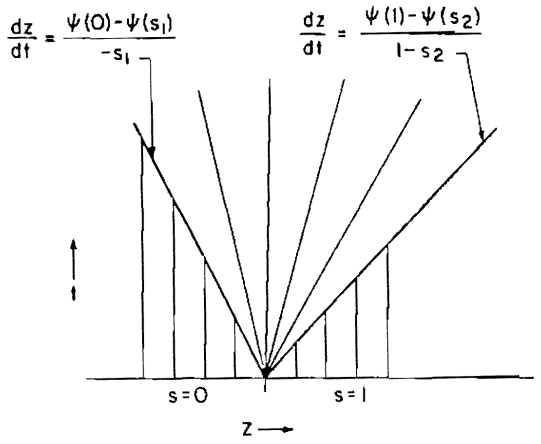

FIG. 4.

rightward travelling shock. Between the two shocks lies an expansion wave, whose fan of characteristics emanates from the initial discontinuity.

Further discussion of the Riemann problem for these equations can be found in [1] and [4].

3.2. Operator splitting for multidimensional problems. For a one-dimensional problem, the system (2.1), (2.2), (2.3) reduces to the single conservation law of the form (3.1), since, in this case, $\mathbf{q}$ is constant in the interior. For a multidimensional problem, a straightforward technique for solving (2.1), (2.2), (2.3) is to solve successively (2.2), (2.3) for p (and $\mathbf{q}$) taking s to be fixed at its approximate solution for the current time, and then to advance (2.1) one time step considering $\mathbf{q}$ fixed, to obtain an approximate solution for s at the new time.

Advancing (2.1) is carried out using the random choice method in [1], [2], and [4] by means of operator splitting. Specifically, for two space dimensions, one solves successively the one-dimensional problems for s

$$\phi \frac{\partial s}{\partial t} + q_x \frac{\partial}{\partial x} f(s) = 0,$$

$$\phi \frac{\partial s}{\partial t} + q_z \frac{\partial}{\partial z} f(s) - \gamma \frac{\partial}{\partial z} g(s) = 0.$$

where $\mathbf{q} = (q_x, q_z)$. Numerical examples can be found in [1], [2], and [4].

Although this technique is efficient and gives acceptable results for many problems of interest, it can be inaccurate for some cases in which a shock front is advancing obliquely to the splitting directions (for example, see [16]). A modification of the split random choice method currently under development overcomes these difficulties and has been shown to give very good results for two space dimensions [9].

4. Front tracking in more than one dimension: SLIC. If one is interested in following the motion of a front in more than one dimension, several techniques are available. One method, mentioned above, is to use the technique of operator splitting to solve appropriate one-dimensional problems along each of the splitting directions in succession until the full multidimensional solution is achieved. In this technique, the location of the front, as such, is never used explicitly. Instead, the movement of the front is implicitly contained in the values of particular variables, in our case, the saturation.

Alternatively, one could choose to concentrate on the line of discontinuity and follow its motion in time. A standard technique is to spread a collection of marker particles along the front at the initial time in such a way that interpolation through these points provides a good approximation to the initial line of discontinuity. From this approximation to the front and the advection velocity

provided by the hyperbolic equations being solved, the direction and speed of the front at each marker particle are determined. Each particle is moved, and interpolation provides the position of the front at the updated time. Of course, the success of the technique relies heavily on the accuracy of the interpolation. Since the direction of motion for each marker particle is obtained, in part, from the orientation of the front at that point, small errors in this orientation can lead to substantial error in the position of the front. In addition, as the marker particles move, they can spread apart as well as bunch together, and it is not a simple task to provide an accurate interpolation to the position of the front from such a collection of points. A discussion of some of the problems inherent in these methods when applied to flame propagation may be found in [31].

As a third alternative, a front tracking method can be based on a "volume of fluid" construction, such as the Simple Line Interface Calculation (SLIC) developed in [26]. In this technique, a grid is imposed on the domain and each cell is assigned a number corresponding to the fraction of that cell located behind the front. These cell fractions are updated during each time step, in accordance with the appropriate differential equations. The position of the front is approximated by a local construction in each cell, based on neighboring cell fractions. This technique does not rely on a global interpretation of the front, and thus can be highly effective in situations in which the front contains fingers and cusps. This method of tracking moving discontinuous fronts is an integral part of a flame propagation algorithm developed in [8], shown to be a natural construction from the point of view of the theory of flame propagation in [31], and used with highly successful results in [32] to model turbulent combustion. Such a method was used in [25] to follow shock discontinuities in Burgers' equation and the equations for two-phase porous flow. In the rest of this section, we discuss SLIC and the application of this type of front tracking method to petroleum reservoir simulations.

4.1. The method. We wish to follow the motion of a front in two space dimensions and assume for now that the velocity at the front is known at all times. We impose a square grid $\{i, j\}$ of uniform mesh size on the domain, and assign a number $0 \leq f_{i,j} \leq 1$ to each cell, corresponding to the fraction of fluid in that cell that is located behind the front. In this discussion, we identify the fluid behind the front as "black" and the fluid ahead as "white." Thus, a cell i,j has volume fraction $f_{i,j} = 1$ if it is entirely behind the front (black), a volume fraction $f_{i,j} = 0$ if it is entirely ahead of the front (white), and $f_{i,j}$ between 0 and 1 if it straddles the front. At any time step, an approximation to the front can be constructed from this array of volume fractions. This interface is advanced under the given velocity field by updating the fractions in the mesh cells in the following manner: The motion of the front is split into a sweep in the x direction with velocity v_x, followed by a sweep in the z direction with velocity v_z, where the

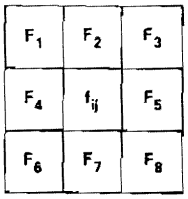

FIG. 5.

velocity of the front is assumed to be (v_x, v_z). For each of these one-dimensional problems, an interface that represents an approximation to the front is drawn in each cell for which $0 < f_{i,j} < 1$. The orientation of the interface depends on the value of $f_{i,j}$ in both the cell and its neighbors. The "black" fluid is then advected in the $x(z)$ direction with velocity $v_x(v_z)$, and the new $f_{i,j}$'s are created, approximating the front advanced a distance $v_x\Delta t(v_z\Delta t)$, where Δt is the time step.

The original algorithm used line segments parallel to either the x- or z-axis to construct the local interface required for the one-dimensional sweeps. Numerous improvements have been made since. Trapezoids were added to the list of possible interface shapes, as well as thin slices of fluid to accommodate fingering. Since interchanging the order of the sweeps produced different results, the question of symmetry arose. One possible solution, of alternating the order of the sweeps, was found to be ineffective. Instead, both contributions were performed, and the new volume fraction in each cell was taken to be the maximum of the two results. This preserved symmetry by removing a bias towards the first sweep present in earlier calculations.

In applying this algorithm to porous flow problems, interfaces oblique to the grid directions were allowed in [25]. As an example of such an interface, consider a cell $f_{i,j}$ with neighbors F_1, F_2, F_3, F_4, F_5, F_6, F_7, and F_8, as in Fig. 5. We assume that the sweep is in the horizontal direction to the right, i.e., $v_x > 0$, and assume that, for example, $F_4 \neq 0$, $F_2 \neq 0$, $F_7 \neq 0$ and $F_5 = 0$. We are interested in establishing the location of the front within the center cell. From these volume fractions, we see that fluid lies on the top, bottom, and left, and thus assume that the front lies roughly parallel to the z-axis, as in Fig. 6. The slope of the interface

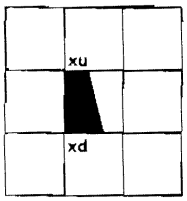

FIG. 6.

is determined from the ratio of the amount of fluid above to the amount of fluid below, namely,

$$\frac{x_u}{x_d} = \frac{F_2}{F_1},$$

and the requirement that the area of the trapezoid equal $f_{i,j}$, i.e.,

$$\tfrac{1}{2}h(x_u + x_d) = h^2 f_{i,j},$$

where x_u and x_d are the length of the sides of the trapezoids as in Fig. 6, and h is the size of the mesh. To advance the front under the time step Δt, we must move the sloped interface under the appropriate velocity field. Let $v_t(v_b)$ be the horizontal velocity at the front along the top (bottom) of the center cell. We translate the nodes of the trapezoid as follows

$$x_u^{n+1/2} = x_u^n + v_t \cdot \Delta t, \qquad x_d^{n+1/2} = x_d^n + v_b \cdot \Delta t,$$

where the superscript $n + \frac{1}{2}$ refers to the result after the first sweep with time step Δt. There are three cases, depending on whether or not the trapezoid has moved into the right cell. In Case 1 (Fig. 7a), the front remains in the center cell, and the updated value of $f_{i,j}$ is easily seen to be

$$f_{i,j}^{n+1/2} = \tfrac{1}{2}h(x_u^{n+1/2} + x_d^{n+1/2}).$$

In Case 2 (Fig. 7b), one leg of the trapezoid has moved to the cell on the right. Letting $\Delta f_{i,j}$ be the amount of fluid that has entered the cell on the right, the center cell is updated to

$$f_{i,j}^{n+1/2} = \tfrac{1}{2}h(x_u^{n+1/2} + x_d^{n+1/2}) - \Delta f_{i,j},$$

while the cell on the right becomes

$$f_{i+1,j}^{n+1/2} = f_{i+1,j}^n + \Delta f_{i,j}.$$

In Case 3, both legs of the trapezoid have moved into the right cell (Fig. 7c), and

$$f_{i,j}^{n+1/2} = 1,$$

while

$$f_{i+1,j}^{n+1/2} = f_{i+1,j}^n + \Delta f_{i,j}.$$

This concludes the one-dimensional sweep for the center cell. The full set of possible interfaces is shown in Fig. 8; the reader is referred to [25] and [32] for details.

Two points are worth mentioning. First, for any given cell, the orientation of the interface in the x sweep may be different from that constructed in the z sweep. Second, for the majority of cells, the value of $f_{i,j}$ and the neighboring $f_{i,j}$'s will be either all 0 or 1, implying that the front is not nearby. In these cases, no

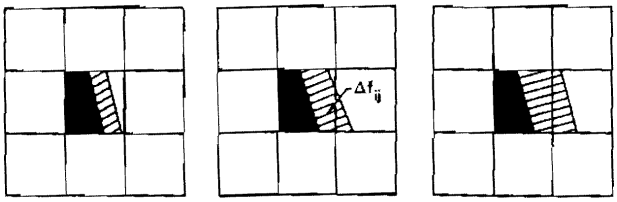

FIG. 7a. FIG. 7b. FIG. 7c.

calculations are required, since the value of $f_{i,j}$ will not change during the movement of the front. Judicious programming can avoid these situations altogether, reducing the calculation from $O(N^2)$ operations to $O(N)$ operations, where N^2 is the number of cells.

4.2. Algorithm for flow through porous media. We now summarize the algorithm presented in [25] for approximating the solution to problems of flow through porous media. The general idea is to use the above front tracking method to follow the discontinuity in s. At each time step, values for the pressure and velocity are obtained from s. This velocity field is used, together with the front tracking method, to move the line of discontinuity and update the saturation parameter.

We consider solving (2.1), (2.2) and (2.3) for the case $\gamma = 0$ (gravity effects absent) for porous flow in a domain Ω. For convenience, we absorb the porosity ϕ

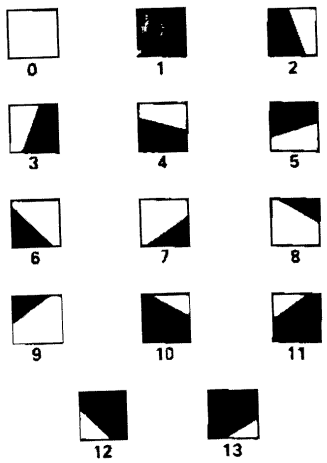

FIG. 8.

into the other variables to obtain

$$\frac{\partial s}{\partial t} + \mathbf{q} \cdot \nabla f(s) = 0, \tag{4.1}$$

$$\nabla \cdot \mathbf{q} = Q, \tag{4.2}$$

$$\mathbf{q} = -\lambda(s)\nabla p\,. \tag{4.3}$$

Let s^n be the value of the saturation at time step $n\Delta t$. We assume that $s^n_{i,j}$ is known at the nodes of a square grid $\{i, j\}$ imposed on Ω. The pressures $p^n_{i,j}$ are taken at the same grid points, and the velocities q_x and q_z will be evaluated at the midpoints of the sides of the cell (see Fig. 9).

We shall describe the algorithm used to obtain $s^{n+1}_{i,j}$ from $s^n_{i,j}$. With $s^n_{i,j}$ known, first $p^n_{i,j}$ is calculated at the grid points. This is accomplished by substituting (4.3) into (4.2) to obtain an expression involving only p and $\lambda(s)$. A finite difference approximation to this expression is then solved, using the known values of $s^n_{i,j}$ to evaluate the necessary coefficient values for λ. Once the values of the pressure $p^n_{i,j}$ have been obtained, a finite difference approximation to (4.3) can be used to produce the velocity field $\mathbf{q}^n = (q^n_x, q^n_z)$.

To move to the next time step, the value of the saturation is updated according to (4.1). We use operator splitting to update s in two steps; a sweep in the x direction followed by a sweep in the z direction. The technique for solving the one-dimensional equation rests on our front tracking algorithm. Given the array of volume fractions $f^n_{i,j}$, we construct an approximation to the front, as described in the previous section. The Rankine–Hugoniot condition (§3) and the values of $\mathbf{q}^n$ and s^n provide the advection speed at the front. We compute the advection speed for all the cells of the front, and transport the black fluid to obtain the new $f^{n+1/2}_{i,j}$. Since we now know both the old and new positions of the front, we can compute the values of $s^{n+1/2}$ away from the front (the continuous parts) by any one of a variety of methods. In [25], both Godunov's method and a random

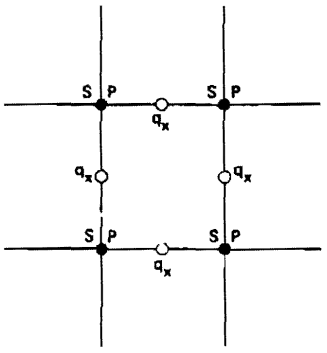

FIG. 9.

choice method are used to advance the solution. Given $s^{n+1/2}$, we complete the iteration by executing the sweep in the z direction, yielding the fully updated s^{n+1}.

4.3. Numerical results. In [25], numerical experiments were carried out for Ω the unit square, with Q corresponding to a source at (0, 0) and a sink at (1, 1), both of unit strength. We describe those experiments here. On $\partial\Omega$ the normal component of $\mathbf{q}$ and the normal derivative of s are both taken to be zero. Initially, the square is occupied entirely by "white" fluid to be displaced (i.e., $s = 0$), except at the point (0, 0) at which $s = 1$. A 40×40 grid was used, with time step small enough so that during one time step, (i) the front can travel at most one cell length and (ii) the waves propagating from individual mesh-point discontinuities do not intersect. At $t = 0$, the square is filled with fluid to be displaced. A source is placed at (0, 0) and a sink at (1, 1), both of unit strength.

For the first test problem, the functions

$$f(s) = \frac{s^2}{s^2 + \alpha(1 - s)^2}, \qquad \lambda(s) = s^2 + \alpha(1 - s)^2$$

were used. This corresponds to a phase mobility proportional to the square of the saturation, and is representative of water flooding of a petroleum reservoir. The quantity α is the ratio of the viscosity of the wetting fluid to that of the nonwetting fluid (such as that of water to oil, respectively). Solutions were calculated for several values of α, corresponding to mobility ratios M at the front

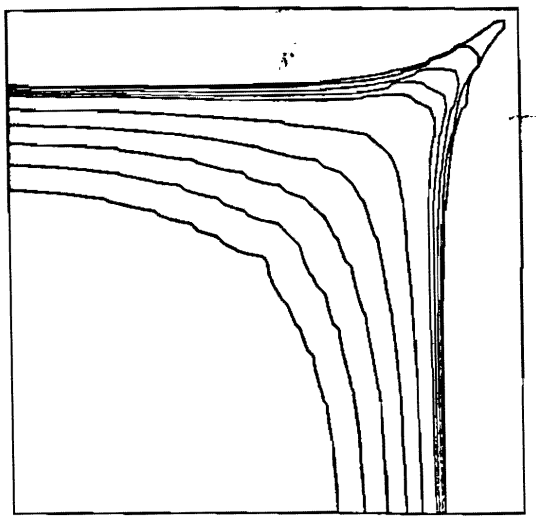

FIG. 10.

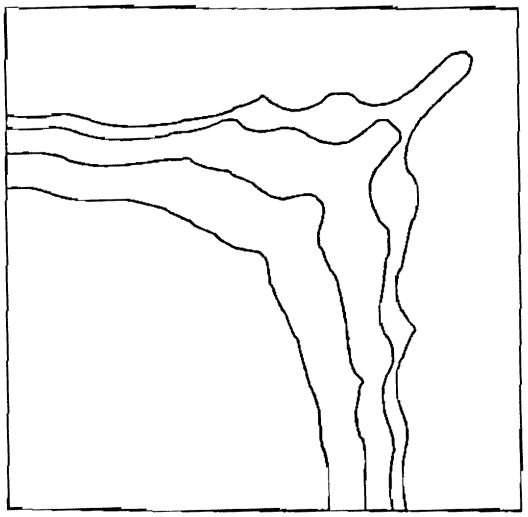

FIG. 11.

in both the stable ($M < 1$) and the unstable ($M > 1$) range. Figure 10 shows the results of a calculation with the above algorithm. With a value of $M = .845$, the front remains stable, as it should, and perturbations die out. In Figure 11, the same equations are solved with $M = 1.397$, a value in the unstable range. In this case, waves develop in the interface and fingering occurs.

The second test problem is one for miscible displacement. For this problem

$$f(s) = s, \quad \lambda(s) = s + M^{-1/4}(1 - s)^4$$

were used. In Fig. 12 we show the results of a calculation with $M = 2$, well into the unstable range. The initial and boundary conditions are the same as in the previous case. The front is unstable, and a "fingering" effect is clearly visible.

5. Godunov-type methods. For a large class of physically interesting cases of flow in porous media (e.g., incompressible flow with negligible capillary pressure), the equations describing the flow can be written as a system of nonlinear hyperbolic conservation laws for the saturations, with an elliptic equation for the total velocity. Solutions to the hyperbolic equations can develop discontinuities, even in cases in which none exist in the initial data. Consequently, it is necessary to use numerical methods that can calculate accurately both continuous and discontinuous solutions. A commonly used class of methods for hyperbolic conservation laws is that of conservative finite difference or finite elements methods. Conservative methods are ones for which the difference equations for the saturations are in discrete divergence form, guaranteeing that the total amount of each component of the fluid is conserved exactly. If the

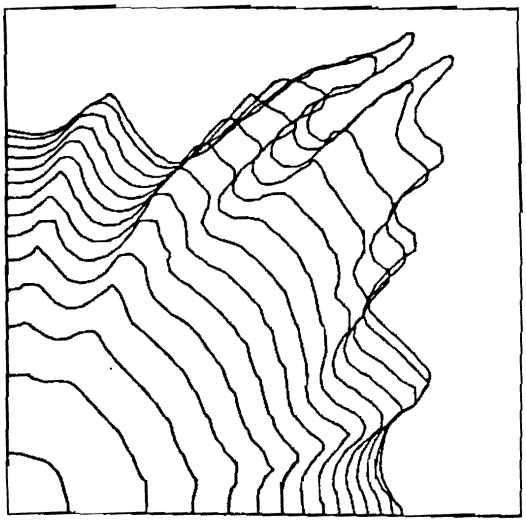

FIG. 12.

method is in discrete divergence form, then discontinuities are constrained to propagate, at least in some average sense, at the correct velocity.

One class of conservative finite difference techniques for calculating discontinuous solutions to systems of hyperbolic conservation laws was introduced by Godunov [19], [20] for gas dynamics. Godunov's method is a generalization to systems of nonlinear equations of the upwind differencing method for scalar advection equations. As such, it is generally too diffusive to represent discontinuities accurately. However, the higher order extensions of Godunov's method, first introduced by van Leer and then developed by a number of authors (for a review, see [22], [36]) have been demonstrated to be effective in calculating complicated time-dependent discontinuous solutions to the equations of gas dynamics in two space dimensions. Consequently, there is reason to believe that these methods will prove useful in calculating solutions to multidimensional problems arising in petroleum reservoir simulation.

We shall discuss the Godunov methods only for the case of one space variable. The one-dimensional form of these methods has been successfully used in multidimensional problems by means of operator splitting [5]. Multidimensional methods that do not require operator splitting are currently under investigation.

5.1. Scalar equations. We consider first Godunov's method for the scalar equation (3.1). We assume that at time t^n we know s_j^n, the average of s across each mesh interval $[(j - \frac{1}{2})\Delta z, (j + \frac{1}{2})\Delta z]$.

$$s_j^n = \frac{1}{\Delta z} \int_{(j-1/2)\Delta z}^{(j+1/2)\Delta z} s(z, t^n)\, dz.$$

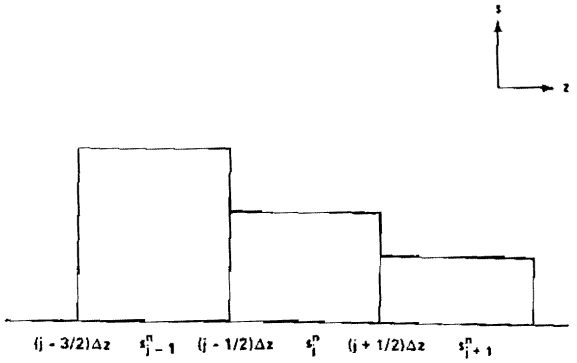

FIG. 13.

In Godunov's method, we interpret the averages s_j^n as giving piecewise constant interpolation functions of the solution in each mesh interval (Fig. 13)

$$s(z, t^n) = s_j^n, \qquad (j - \tfrac{1}{2})\Delta z < s < (j + \tfrac{1}{2})\Delta z. \tag{5.1}$$

Since we know the solution to the Reimann problem, we can solve the initial value problem given by (5.1) exactly (Fig. 14), for a time Δt sufficiently small so that the waves from successive Riemann problems do not intersect. We denote the exact solution by $s_e^n(z, t)$. In order to obtain s_j^{n+1}, the average of the solution at the new time, we average $s_e^n(z, t)$ over the jth mesh interval (Fig. 15)

$$s_j^{n+1} = \frac{1}{\Delta z}\int_{(j-1/2)\Delta z}^{(j+1/2)\Delta z} s_e^n(z, t^n + \Delta t)\, dz. \tag{5.2}$$

If the solution has complicated spatial structure, the evaluation of the integral in

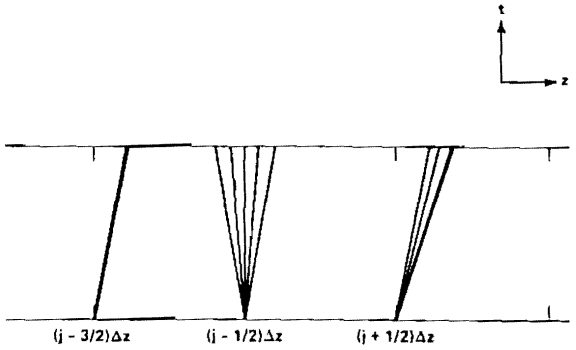

FIG. 14.

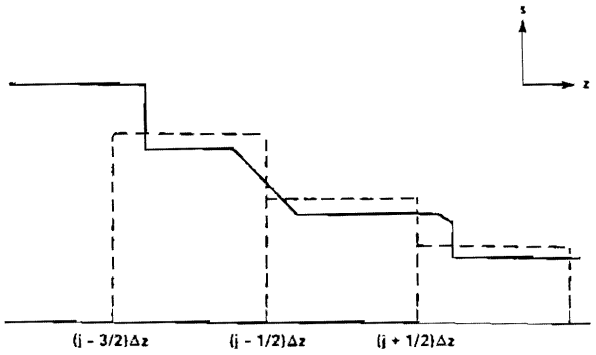

FIG. 15.

(5.2) can be difficult. By applying the divergence theorem to

$$\int_{(j-1/2)\Delta z}^{(j+1/2)\Delta z} \int_{t^n}^{t^n+\Delta t} \left(\frac{\partial s}{\partial t} + \frac{\partial \psi}{\partial z}\right) dt\, dz,$$

we obtain a difference formula for s_j^{n+1}.

$$(5.3)\quad s_j^{n+1} - s_j^n = \frac{1}{\Delta z} \int_{t^n}^{t^n+\Delta t} (\psi(s_e^n((j-\tfrac{1}{2})\Delta z, t)) - \psi(s_e^n((j+\tfrac{1}{2})\Delta z, t)))\, dt.$$

We observe that $s_e^n((j+\frac{1}{2})\Delta z, t) = s_{j+1/2}^{n+1/2}$, independent of t, where $s_{j+1/2}^{n+1/2}$ is obtained by evaluating the solution to the Riemann problem for (3.1) along the ray $(z-(j-\frac{1}{2})\Delta z)/(t-t^n) = 0$, with left and right states s_j^n, s_{j+1}^n. Thus we obtain

$$(5.4)\qquad s_j^{n+1} = s_j^n + \frac{\Delta t}{\Delta z}(\psi(s_{j-1/2}^{n+1/2}) - \psi(s_{j+1/2}^{n+1/2})).$$

The scheme is first order accurate, and is stable if $(\Delta t/\Delta z)\max_j|\psi'(s_j^n)| \leqq 1$.

We now restrict our example further, by assuming $\psi'(s) \geqq 0$, for all s. The solution to the Riemann problem at $(z-(j-\frac{1}{2})\Delta z)/(t-t^n) = 0$ is always the left state, implying that $s_{j+1/2}^{n+1/2} = s_j^n$ in (5.4). Thus Godunov's method in this situation reduces to upwind differencing, which is excessively dissipative. To obtain an algorithm with less dissipative error we replace the piecewise constant interpolation function (5.1) with one that is more accurate, and use the wave propagation properties of the equation to derive a difference scheme of the form (5.4).

The simplest such interpolation function we might use is a piecewise linear interpolation function (Fig. 16)

$$(5.5)\qquad s(z,t^n) = s_j^n + \delta s_j \frac{(z-j\Delta z)}{\Delta z}, \qquad (j-\tfrac{1}{2})\Delta z < z < (j+\tfrac{1}{2})\Delta z,$$

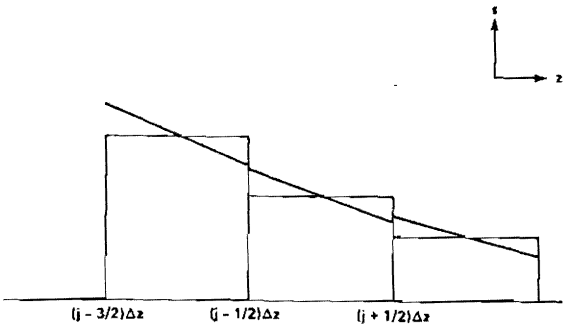

FIG. 16.

where $\delta s_j/\Delta z$ approximates $\partial s/\partial z|_{j\Delta z}$, subject to some constraints described below. Unlike the case for the piecewise constant interpolant, it is difficult to solve the piecewise linear problem analytically. Consequently, the difference scheme for the piecewise linear case is derived by approximating the time integrals in (5.3). If we approximate them using the midpoint rule, we obtain

$$s_j^{n+1} \approx s_j^n + \frac{\Delta t}{\Delta z}\left[\psi(s_c^n((j-\tfrac{1}{2})\Delta z, t^n + \tfrac{1}{2}\Delta t)) - \psi(s_c^n((j+\tfrac{1}{2})\Delta z, t^n + \tfrac{1}{2}\Delta t))\right].$$

We then approximate the value $s_c^n((j-\frac{1}{2})\Delta z, t^n + \frac{1}{2}\Delta t)$ by using the fact that solutions to (3.1) are constant along characteristics. If we approximate the characteristic through $((j+\frac{1}{2})\Delta z, t^n + \frac{1}{2}\Delta t)$ by the straight line (Fig. 17)

$$z(t) = (j+\tfrac{1}{2})\Delta z + (t - (t^n + \tfrac{1}{2}\Delta t))\psi'(s_j^n),$$

we obtain, using our interpolation function (5.5)

$$s_c^n((j+\tfrac{1}{2})\Delta z, t^n + \tfrac{1}{2}\Delta t) \approx s((j+\tfrac{1}{2})\Delta z - \tfrac{1}{2}\Delta t\,\psi'(s_j^n), t^n)$$
$$= s_j^n + \frac{1}{2}\left(1 - \frac{\Delta t}{\Delta z}\psi'(s_j^n)\right)\delta s_j.$$

Collecting the approximations, we obtain the difference scheme

$$s_j^{n+1} = s_j^n + \frac{\Delta t}{\Delta z}(\psi(s_{j-1/2}^{n+1/2}) - \psi(s_{j+1/2}^{n+1/2})),$$
$$s_{j+1/2}^{n+1/2} = s_j^n + \frac{1}{2}\left(1 - \frac{\Delta t}{\Delta z}\psi'(s_j^n)\right)\delta s_j. \tag{5.6}$$

To complete the specification of the scheme, we need to define δs_j. It is defined in two steps. First, we calculate a preliminary value $\widetilde{\delta s}_j$ using a central difference formula, e.g., $\frac{1}{2}\widetilde{\delta s}_j = s_{j+1} - s_{j-1}$ (for other examples, see [11], [35]). We then

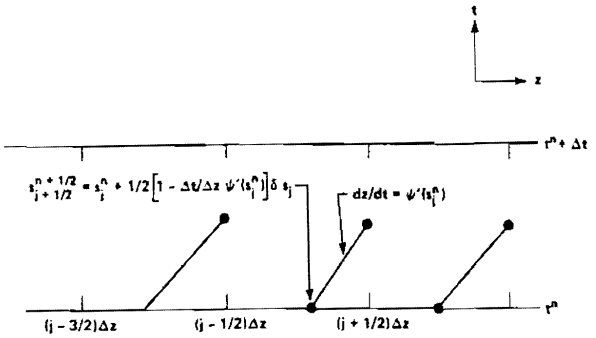

FIG. 17.

obtain our final value for δs_j by constraining $\tilde{\delta} s_j$ to be within certain bounds. The purpose of the constraints is to prevent overshoots and undershoots at discontinuities. For example, the dashed profile in Fig. 18 represents a piecewise linear interpolant for which the left extrapolated value is out of the range defined by the adjacent zone averages. In that case, the slope is reduced so that the extrapolated value lies just within range, as represented by the dotted line. Also, if a zone average is a local extremum, then δs_j is set to zero. Expressed quantitatively, these constraints are given by

$$\delta s_j = \begin{cases} \min(|\tilde{\delta} s_j|, 2|s_{j+1} - s_j|, 2|s_j - s_{j-1}|)\ \text{sign}\ (s_{j+1} - s_{j-1}) \\ \qquad \text{if } (s_{j+1} - s_j)(s_j - s_{j-1}) > 0, \\ 0 \qquad \text{otherwise.} \end{cases} \tag{5.7}$$

In smooth parts of the solution, these inequalities are already satisfied by $\tilde{\delta} s_j$, so that $\delta s_j = \tilde{\delta} s_j$. With this choice of δs_j, it is not difficult to show that, if the solution is smooth, the scheme is formally second-order accurate.

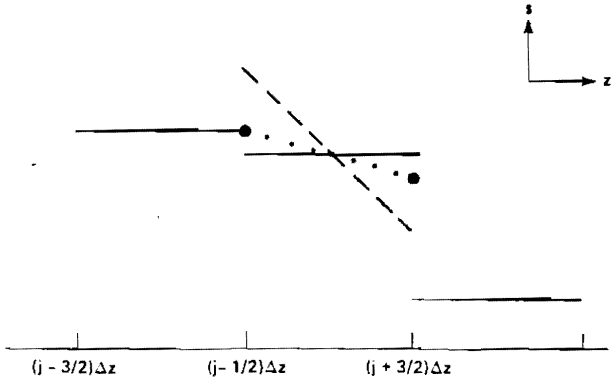

FIG. 18.

A numerical comparison between the first-order and second-order Godunov methods is depicted in Figs. 19 and 20. For these problems $s(z, t) = 1$ for $0 \leq z \leq 0.2$ and $s(z, 0) = 0$ for $0.2 < z \leq 1$. The dashed curves represent the solution of (3.1) with $\psi(s) = f(s) = s^2/(s^2 + 0.5(1 - s)^2)$ and $\Delta z = 0.02$. The first order method is depicted in Fig. 19 and the second order one in Fig. 20. The

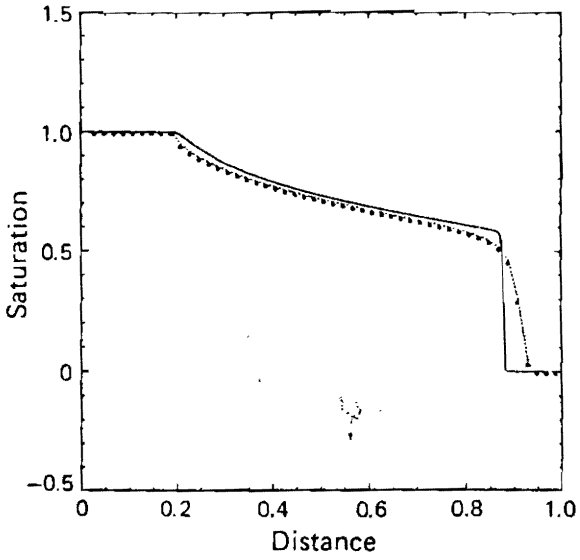

FIG. 19.

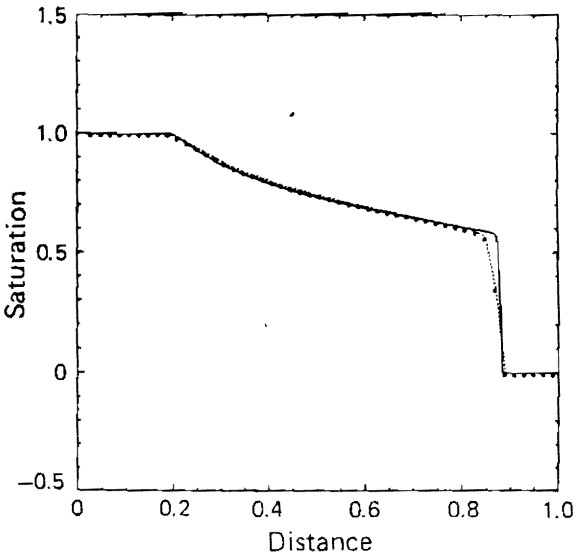

FIG. 20.

plotting routine indicates the data points by placing circles below them, more or less tangent to the interpolating curve. The solid lines in the figures represent the solution for $\Delta z = 0.0025$ using the second order method, which is essentially the exact solution for this case (data points are not indicated). The time step Δt was taken to be $0.1\ \Delta z$ for all cases, which corresponds to a CFL number of about 0.2. The improvement in the solution using the second-order over the first-order method is easily seen for this problem.

5.2. Systems of equations. We wish to extend the techniques described above to the case of the initial value problem for systems of hyperbolic conservation laws in one space variable

$$\begin{aligned} &\frac{\partial U}{\partial t} + \frac{\partial F(U)}{\partial z} = 0, \\ &U(z,t) = U: \mathbb{R} \times [0,T] \to \mathbb{R}^N, \\ &F(U) = F: \mathbb{R}^N \to \mathbb{R}^N, \qquad U(z,0) = U_0(z) \text{ given.} \end{aligned} \tag{5.8}$$

In porous flow problems, U might be a vector of saturations, and $F(U)$ the vector of associated fractional flows. The system is assumed to be hyperbolic, i.e., the matrix $\nabla_U F = A(U)$ has N real eigenvalues $\lambda_1(U) < \cdots < \lambda_N(U)$ with corresponding left and right eigenvectors $(l_1, r_1), \cdots, (l_N, r_N)$. These eigenvectors are linearly independent and biorthogonal, i.e., $l_i \cdot r_j = 0$ if $i \neq j$. If one expands an arbitrary vector W in terms of the r_k's, then it follows from the biorthogonality property that the expansion coefficients are given by

$$W = \sum_{k=1}^{N} \alpha_k r_k, \qquad \alpha_k = l_k \cdot W.$$

These eigenvectors and eigenvalues are used to describe the infinitesimal wave propagation properties of the system (5.8). The characteristic curves of (5.8) are curves in (z, t) satisfying the ordinary differential equations

$$\frac{dz_k}{d\sigma_k} = \lambda_k(U(z_k(\sigma_k), t_k(\sigma_k))), \qquad \frac{dt_k}{d\sigma_k} = 1, \qquad k = 1, \cdots, N. \tag{5.9}$$

In regions where the solution is not discontinuous, a solution to (5.1) satisfies for each k an ordinary differential equation along the kth characteristic curve

$$l_k \cdot \frac{d}{d\sigma_k}(U(z_k(\sigma_k), t_k(\sigma_k))) = 0, \qquad k = 1, \cdots, N. \tag{5.10}$$

Derivatives of the solution are transported along characteristics, the component of the derivative transported along the kth characteristic being proportional to r_k.

As in the scalar case, we assume that U_j^n, the average value of the solution across a mesh interval, is known at time t^n

$$U_j^n = \frac{1}{\Delta z}\int_{(j-1/2)\Delta z}^{(j+1/2)\Delta z} U(z, t^n)dz.$$

We then wish to calculate U_j^{n+1}, the average value of the solution at time $t^n + \Delta t$. As in the scalar case above, we do so in the following three steps: (i) interpolate piecewise linear approximations to the solution at time t^n; (ii) use the wave propagation properties of the solution, in the form of Riemann problems and characteristic equations to find approximate values $U_{j+1/2}^{n+1/2}$ to the solution at $((j + \frac{1}{2})\Delta z, t^n + \frac{1}{2}\Delta t)$; and (iii) perform a conservative finite difference step to find U_j^{n+1}, of the form

$$U_j^{n+1} = U_j^n + \frac{\Delta t}{\Delta z}\left(F\left(U_{j-1/2}^{n+1/2}\right) - F\left(U_{j+1/2}^{n+1/2}\right)\right). \tag{5.11}$$

Steps (i) and (ii) are at the heart of the method. In these two steps, we generalize the algorithm given above for scalar equations by applying it one mode of wave propagation at a time, using the characteristic equations (5.9), (5.10). Since the characteristic form of the equations breaks down at shocks, care is required to guarantee that the algorithm reverts to something well-behaved near shocks.

The interpolation step is a straightforward generalization of what was done in the scalar case, except that the constraints are imposed in characteristic variables. We first calculate the preliminary value for the slope $\delta\tilde{U}_j = \frac{1}{2}(U_{j+1} - U_{j-1})$. We then modify the slope, using Harten's monotonicity algorithm for characteristic variables [21]. We expand

$$2\left(U_{j+1} - U_j\right) = \sum_{k=1}^{N} \bar{\alpha}_k^R r_k\left(U_j\right),$$

$$2\left(U_j - U_{j-1}\right) = \sum_{k=1}^{N} \bar{\alpha}_k^L r_k\left(U_j\right),$$

$$\delta\tilde{U}_j = \sum_{k=1}^{N} \tilde{\alpha}_k r_k\left(U_j\right).$$

We then define

$$\alpha_k = \begin{cases} \min(|\bar{\alpha}_k^L|, |\bar{\alpha}_k^R|, |\tilde{\alpha}_k|) \times \operatorname{sign}(\tilde{\alpha}_k) & \text{if } \bar{\alpha}_k^L \cdot \bar{\alpha}_k^R > 0, \\ 0 & \text{otherwise.} \end{cases}$$

The constrained slope is then given by

$$\delta U_j = \sum \alpha_k r_k(U_j).$$

Given these interpolated profiles, we can now calculate $U_{j+1/2}^{n+1/2}$. The difficulty

in calculating $U_{j+1/2}^{n+1/2}$ is that we want two rather different answers in two different limits.[1] In smooth parts of the solution we want $U_{j+1/2}^{n+1/2}$ to satisfy a finite difference approximation to the characteristic form of the equations (5.9), (5.10), i.e., we want it to satisfy the N linear equations

$$l_k \cdot (U_{j+1/2}^{n+1/2} - U_{j+1/2,k}), \qquad k = 1, \cdots, N,$$

where $U_{j+1/2,k}$ is the value of the solution at the base of the kth characteristic and is given by

$$U_{j+1/2,k} = \begin{cases} U_j^n + \frac{1}{2}\left(1 - \frac{\Delta t}{\Delta z}\lambda_k\right)\delta U_j & \text{if } \lambda_k > 0, \\ U_{j+1}^n - \frac{1}{2}\left(1 + \frac{\Delta t}{\Delta z}\lambda_k\right)\delta U_j & \text{if } \lambda_k < 0. \end{cases}$$

In the case for which $(j + \frac{1}{2})\Delta z$ is inside a discontinuity, our interpolated profile may look like the profile in Fig. 21, due to the constraints on δU. In that case, we want our solution $U_{j+1/2}^{n+1/2}$ to be given by the Riemann problem with left and right states corresponding to the jump at $(j + \frac{1}{2})\Delta z$, plus some perturbation representing the slopes on either side. One algorithm for $U_{j+1/2}^{n+1/2}$ that has the appropriate behavior is given in [13] for gas dynamics, but extends easily to this more general context.

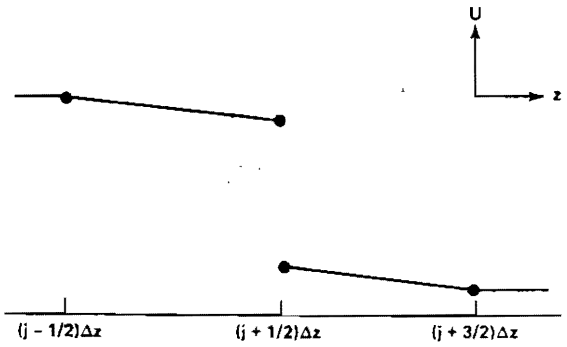

FIG. 21.

We take $U_{j+1/2}^{n+1/2}$ to be the solution to the Riemann problem with left and right states $U_{j+1/2,L}$, $U_{j+1/2,R}$, given by

$$\begin{aligned} U_{j+1/2,L} &= U_{j+1/2,L}^n - A_{j+1/2,L}\,\delta U_j, \\ U_{j+1/2,R} &= U_{j+1/2,R}^n - A_{j+1/2,R}\,\delta U_{j+1}. \end{aligned} \tag{5.12}$$

[1] In the scalar results presented above, we avoided this problem by assuming $\psi'(s) \geq 0$.

Here $U^n_{j+1/2,L} = U^n_j + \frac{1}{2}\delta U_j$, $U^n_{j+1/2,R} = U^n_{j+1} - \frac{1}{2}\delta U_{j+1}$, and the operators $A_{j+1/2,L}$, $A_{j+1/2,R}$ are sums of the characteristic projection operators

$$A_{j+1/2,L}W = \sum_{k:\lambda_k(U^n_j)>0} \frac{1}{2}\lambda_k(U^n_j)\frac{\Delta t}{\Delta z}(l_k(U^n_j)\cdot W)r_k(U^n_j),$$

$$A_{j+1/2,R}W = \sum_{k:\lambda_k(U^n_{j+1})<0} \frac{1}{2}\lambda_k(U^n_{j+1})\frac{\Delta t}{\Delta z}(l_k(U^n_{j+1})\cdot W)r_k(U^n_{j+1}).$$

The vector $U_{j+1/2,L}$ ($U_{j+1/2,R}$) is equal to the left (right) limiting value of U at $((j+\frac{1}{2})\Delta z, t^n)$ plus the amount of wave of each family contained in $\delta U_j(\delta U_{j+1})$ that can reach $(j+\frac{1}{2})\Delta z$ from the left (right) between time t^n and $t^n + \frac{1}{2}\Delta t$. If $|\delta U_j|, |\delta U_{j+1}| \ll |U_j - U_{j+1}|$, then it is clear from (5.12) that $U^{n+1/2}_{j+1/2}$ is given by a small perturbation of the solution to the Riemann problem. If the solution is smooth, then it is not difficult to show that $U^{n+1/2}_{j+1/2}$ approximates, to second order, a solution to the characteristic equations (5.9), (5.10). This follows from the fact that, for weak waves, the solution to the Riemann problem reduces to transport along characteristics.

Throughout this discussion, we have assumed that the Riemann problem for (5.1) could be easily solved. In fact, this has been shown to be the case for only a few of the systems of equations arising in multiphase flow in porous media [23], [34], [35]. However, it is possible to introduce approximations into the solution of the Riemann problem without loss of accuracy, since much of the information in the Riemann problem is lost in the conservative differencing step. In particular, a class of approximate solutions is proposed in [30], and an explicit constructive algorithm for such approximate solutions for general systems of conservation laws is given in [12]. This class of approximate solutions is accurate in two limiting cases: if all the waves in the solution are weak, or if the solution consists of a single strong wave. For incompressible flow in porous media, these are the two most common situations since the magnitude and the direction in U-space of the jumps across waves are independent of the direction of propagation of the wave.

Acknowledgments. This work was supported in part by the Director, Office of Energy Research, Office of Basic Energy Sciences, Engineering, Mathematical, and Geosciences Division of the U.S. Department of Energy under contract DE-AC03-76SF00098.

REFERENCES

[1] N. ALBRIGHT, C. ANDERSON, AND P. CONCUS, *The random choice method for calculating fluid displacement in a porous medium*, Boundary and Interior Layers—Computational and Asymptotic Methods, J.J.H. Miller, ed., Boole Press, Dublin, 1980, pp. 3–13.

[2] N. ALBRIGHT AND P. CONCUS, *On calculating flows with sharp fronts in a porous medium*, Fluid Mechanics in Energy Conservation, J. D. Buckmaster, ed., Society for Industrial and Applied Mathematics, Philadelphia, 1980, pp. 172–184.

[3] N. ALBRIGHT, P. CONCUS, AND W. PROSKUROWSKI, *Numerical solution of the multidimensional Buckley–Leverett equation by a sampling method*, SPE 7681, 5th SPE Symposium on Reservoir Simulation, Denver, 1979.

[4] C. ANDERSON AND P. CONCUS, *A stochastic method for modeling fluid displacement in petroleum reservoirs*, in Analysis and Optimization of Systems, A. Bensoussan and J. L. Lions, eds., Lecture Notes in Control and Information Sciences 28, Springer-Verlag, Berlin, pp. 827–841.

[5] J. B. BELL, P. COLELLA, P. CONCUS, AND H. GLAZ, *Higher order Godunov methods for the Buckley-Leverett equation*, presented at SIAM 30th Anniversary Meeting, Stanford, CA, 1982.

[6] A. J. CHORIN, *Random choice solution of hyperbolic systems*, J. Comp. Phys., 22 (1976), pp. 517–533.

[7] ———, *Random choice methods with applicatons to reacting gas flow*, J. Comp. Phys., 25 (1977), pp. 253–272.

[8] ———, *Flame advection and propagation algorithms*, J. Comp. Phys., 35 (1980), pp. 1–11.

[9] ———, *Instability of fronts in a porous medium*. Report LBL-15893, Lawrence Berkeley Lab., Univ. California, Berkeley 1983; Comm. Math. Phys., to appear.

[10] P. COLELLA, *Glimm's method for gas dynamics*, SIAM J. Sci. Statist. Comput., 3 (1982) pp. 76–110.

[11] ———, *A direct Eulerian* MUSCL *scheme for gas dynamics*, Report LBL-14014, Lawrence Berkeley Lab., Univ. California, Berkeley 1982; SIAM J. Sci. Stat. Comput., to appear.

[12] ———, *Approximate solution of the Riemann problem for real gases*. Report LBL-14442, Lawrence Berkeley Lab., Univ. California, Berkeley 1983; J. Comp. Phys., to appear.

[13] P. COLELLA AND P. R. WOODWARD, *The piecewise-parabolic method* (PPM) *for gas-dynamical simulations*, Report LBL-14661, Lawrence Berkeley Lab., Univ. California, Berkeley, 1983; J. Comp. Phys., to appear.

[14] P. CONCUS, *Calculation of shocks in oil reservoir modeling and porous flow*, in Numerical Methods for Fluid Dynamics, K. W. Morton and M. J. Baines, eds., Academic Press, New York, 1982, pp. 165–178.

[15] P. CONCUS AND W. PROSKUROWSKI, *Numerical solution of a nonlinear hyperbolic equation by the random choice method*, J. Comp. Phys., 30 (1979), pp. 153–166.

[16] M. CRANDALL AND A. MAJDA, *The method of fractional steps for conservation laws*, Numer. Math., 34 (1980), pp. 285–314.

[17] J. GLIMM, *Solutions in the large for nonlinear hyperbolic systems of equations*, Comm. Pure Appl. Math., 18(1965), pp. 697–715.

[18] J. GLIMM, D. MARCHESIN AND O. MCBRYAN, *The Buckley–Leverett equation: theory, computation and application*, Proc. Third Meeting of the International Society for the Interaction of Mechanics and Mathematics, Edinburgh, 1979; Trends in Applications of Pure Mathematics in Mechanics, R. J. Knops, ed., Edinburgh, 1979.

[19] S. K. GODUNOV, *Finite difference methods for numerical computation of discontinuous solutions of the equations of fluid dynamics*. Mat. Sbornik, 47 (1959), pp. 271–306. (In Russian.)

[20] S. K. GODUNOV, A. V. ZABRODYN, AND G. P. PROKOPOV, *A computational scheme for two-dimensional nonstationary problems of gas dynamics and calculations of the flow from a shock wave approaching a stationary state*, USSR Comput. Math. Math. Phys., 1 (1961), pp. 1187–1218.

[21] A. HARTEN, *On second order accurate Godunov-type schemes*, preprint, 1982.

[22] A. HARTEN, P. D. LAX, AND B. VAN LEER, *On upstream differencing and Godunov-type schemes for hyperbolic conservation laws*, SIAM Rev., 25 (1983), pp. 35–62.

[23] E. ISAACSON, *Global solution of a Riemann problem for a non-strictly hyperbolic system of conservation laws arising in enhanced oil recovery*, preprint, Math. Dept., Rockefeller Univ., New York, 1982; J. Comp. Phys., to appear.

[24] P. D. LAX, *Hyperbolic Systems of Conservation Laws and the Mathematical Theory of Shock Waves*, CBMS Regional Conference Series in Applied Mathematics 11, Society for Industrial and Applied Mathematics, Philadelphia, 1973.

[25] P. LOTSTEDT, *A front tracking method applied to Burgers' equation and two-phase porous flow*, J. Comp. Phys., 47 (1982), pp. 211–228.

[26] W. F. NOH AND P. WOODWARD, SLIC (*Simple Line Interface Calculation*), Proc. 5th Intl. Conference on Numerical Methods in Fluid Dynamics, A. I. van de Vooren and P. J. Zandbergen, eds., Lecture Notes in Physics 59, Springer-Verlag, Berlin, 1976, pp. 330–340.

[27] O. A. OLEINIK, *Uniqueness and stability of the generalized solution of the Cauchy problem for a quasilinear equation*, AMS Translat., Ser. 2, 33 (1963), pp. 285–290.

[28] D. W. PEACEMAN, *Fundamentals of Numerical Reservoir Simulation*, Elsevier, Amsterdam, 1977.

[29] W. PROSKUROWSKI, *A note on solving the Buckley–Leverett equation in the presence of gravity*, J. Comp. Phys., 41 (1981), pp. 136–141.

[30] P. ROE, *Approximate Riemann solvers, parameter vectors, and difference schemes*, J. Comp. Phys., 43 (1981), pp. 357–372.

[31] J. A. SETHIAN, *An analysis of flame propagation*, Report LBL-14125, Lawrence Berkeley Lab., Univ. California, Berkeley, 1982.

[32] ———, *Turbulent combustion in open and closed vessels*, Report LBL-15744, Lawrence Berkeley Lab., Univ. California, Berkeley, 1983; J. Comp. Phys. (1984), to appear.

[33] B. TEMPLE, *Global solution for the Cauchy problem for a class of* 2×2 *nonstrictly hyperbolic conservation laws*, Adv. Appl. Math, 3 (1983), pp. 335–375.

[34] ———, *Systems of conservation laws with coinciding shock and rarefaction curves*, preprint; Proc. Amer. Math. Soc, to appear.

[35] B. VAN LEER, *Towards the ultimate conservative difference scheme. V. A second-order sequel to Godunov's method*, J. Comp. Phys., 32 (1979), pp. 101–136.

[36] P. R. WOODWARD AND P. COLELLA, *The numerical simulation of two-dimensional fluid flow with strong shocks*, J. Comp. Phys, to appear.